Corrosion inhibition of WE43 Mg alloy by salicylic compounds: Influence of nitro substitution

François-Xavier Perrin, Nadja Leibl, Lénaïk Belec, Armand Fahs, Nicolas Caussé, Nadine Pébère

Corrosion Science 242 (2025) 112558

Contents lists available at ScienceDirect

Corrosion Science

journal homepage: www.elsevier.com/locate/corsci

Corrosion inhibition of WE43 Mg alloy by salicylic compounds: Influence of nitro substitution

François-Xavier Perrin [a,*], Nadja Leibl [a], Lénaïk Belec [a], Armand Fahs [a], Nicolas Caussé [b], Nadine Pébère [b,*]

[a] MAPIEM, Université de Toulon, CS 60584, Cedex 9, Toulon 83041, France
[b] CIRIMAT, Toulouse INP, Université Toulouse 3 Paul Sabatier, CNRS, Université de Toulouse, 4 allée Emile Monso - BP44362, Cedex 4, Toulouse 31030, France

ARTICLE INFO

Keywords:
Mg-RE magnesium alloys
Corrosion inhibitors
NaCl solution
Electrochemistry
Hydroxo-complexes

ABSTRACT

The corrosion inhibition of WE43 Mg alloy by salicylic acid (SA) and 3,5-dinitrosalicylic acid (DNSA) was investigated in a 0.2 M NaCl solution using electrochemical techniques, pH measurements, inductive coupled plasma-optical emission spectroscopy (ICP-OES) and SEM-EDX analyses. SA has a poor performance while DNSA was efficient after some hours of immersion in the NaCl solution. The observed behaviour was attributed, for short immersion times, to a buffering effect of DNSA which delayed the $Mg(OH)_2$ crystal growth on the alloy surface, and for longer immersion times, to an enrichment of the corrosion products layer by the alloying elements.

1. Introduction

Due to their high strength-to-weight ratio, Mg alloys are good candidates for applications where weight savings are vital, particularly in the automotive, aerospace and mobile electronics. However, their poor corrosion and wear resistances limit the potential of using Mg alloys in these fields of application. A wide variety of protecting strategies has been investigated, including alloying [1], chemical conversion coatings [2,3] and use of inhibitors [2], added directly to the aggressive solution or incorporated into organic or inorganic coatings [3,4]. Less conventional techniques, such as ion implantation, have also shown to be effective to delay Mg alloys degradation. For example, enhanced corrosion resistance of Nd-implanted WE43 Mg alloy has been attributed to the combination of an outer stable and protective Nd_2O_3 layer and an inner partially protective MgO layer [5].

Inorganic and organic inhibitor systems for Mg alloys have been the subject of recent reviews [2,6]. It is worth noting that inhibition mechanisms for Mg and Mg alloys would be different from those observed with other metals. For example, Wang et al. [7] have shown that the inhibitory effect of benzotriazole (BTA) differed from that observed on Cu or Cu-bearing alloys. The corrosion resistance of a Mg-Zn-Al-Mn-Ca alloy in 0.1 M NaCl and for a pH value of 10 was greatly enhanced by the addition of a high BTA concentration (15 g/L). This high degree of protection has been associated with the formation of a dense and highly crystalline $Mg(OH)_2$ layer. The authors assumed that the adsorbed BTA^- anion (the predominant form of BTA at pH = 10) acted as a nucleation site for the formation of this layer. The inhibition mechanism of vanadate salts for AZ31 Mg alloy also appeared different from that observed for the AA2024-T3 alloy [8]. This different film-forming mechanism has been linked to the reductive adsorption process that accompanies film formation on AZ31.

The pH of the solution also impacts the inhibition efficiency. For instance, phosphates are more effective in acidic or neutral media than in alkaline media, because in the latter case $Mg_3(PO_4)_2$ precipitation occurs in solution rather than in the vicinity of local cathodic sites [9]. The most common mode of action of organic corrosion inhibitors for Mg and its alloys is the formation of insoluble complexes between Mg^{2+} ions and the inhibitor (for example, sodium di-octylphosphate [10], alkyl carboxylates [11], 2-hydroxy-4-methoxy-acetophenone [12], 5,10,15, 20-tetraphenylporphyrin [13], 8-hydroxyquinoline [14]). They have the effect of blocking porosities in the $Mg(OH)_2$ layer. An inhibition mechanism by adsorption has been reported for surfactants with carboxylic [11], sulfate [15] or sulfonates [16] hydrophilic heads. However, inhibition by precipitation of insoluble complexes is more common than inhibition by adsorption on Mg surface. A new inhibition mechanism has recently been proposed by Cui et al. [17], according to which anionic inhibitors, such as sodium dodecyl sulfate, by electrostatically adsorbing onto $Mg(OH)_2$ embryos, promote crystal nucleation and

* Corresponding authors.
E-mail addresses: perrin@univ-tln.fr (F.-X. Perrin), nadine.pebere@toulouse-inp.fr (N. Pébère).

https://doi.org/10.1016/j.corsci.2024.112558
Received 7 August 2024; Received in revised form 15 October 2024; Accepted 4 November 2024
Available online 14 November 2024

enable the formation of a denser, more protective corrosion product film.

Numerous examples have also shown that the inhibitor efficiency depends closely on the specific composition of the Mg alloy [2].

Magnesium alloys containing rare-earth (RE) and Zr addition elements have improved mechanical properties up to 300 °C and good resistance to ignition [18,19]. The WE43 Mg alloy is characterized by intermetallics enriched in RE (mainly Y and Nd) and Zr elements. Generally, these intermetallics are reported to act as local cathodes [20–22]. However, Feng et al. [23] have recently shown that the RE-rich intermetallics acted as microanodes in a Na_2SO_4 solution. The incorporation of alloying elements, mainly yttrium and zirconium, in the corrosion product layer has an impact on the corrosion rate [20,24]. For example, Leleu et al. [20] have studied the corrosion resistance of three Mg alloys containing rare-earth elements (WE43, EV31 and ZE41) and that of two Mg-Al alloys (AZ31 and AZ91). From inductive coupled plasma-optical emission spectroscopy and from electrochemical measurements, higher corrosion rates were observed for the rare-earth Mg alloys compared to the AZ series alloys.

Anodizing treatments, such as electrolytic plasma in an alkaline phosphate solution, confer limited protection for the WE43 Mg alloy compared with the AZ91D alloy in a 3.5 wt% NaCl medium [25]. Chemical conversion treatments of the WE43 Mg based with cerium salts (sulphate and chloride) did not provide any significant protection [26]. However, in the form of an organic cerium phosphate (cerium tri (bis-2ethylhexyl)phosphate) incorporated in a thin epoxy-silane coating, it has confered a self-healing ability to the coating [27]. Molybdate ions lead to contrasting results, with a corrosion-accelerating effect for a wide variety of industrial Mg alloys (including the WE43) in 0.5 wt% NaCl medium at a concentration of 50 mM [2], whereas a strong inhibiting effect was demonstrated at a higher concentration (100 mM) for the WE43 in 0.05 M NaCl medium [28]. In the latter case, it was shown that Na_2MoO_4 inhibits corrosion while forming a protective mixed-valence Mo(VI)-Mo(V) layer that prevents further corrosion attack.

Among the 151 compounds evaluated by Lamaka et al. [2] (results re-discussed recently by Cui et al. [17]) to inhibit corrosion of Mg alloys and pure Mg in NaCl media, salicylate derivatives appeared particularly promising. Moreover, studies conducted in recent years on iron-rich Mg alloys have demonstrated a dual effect based on the formation of soluble Fe^{3+}/salicylate complexes, that inhibited iron redeposition, and on the stabilization of $Mg(OH)_2$ nanocrystals [29,30]. A noticeable effect of the Fe content in Mg has been observed with salicylate, with no inhibition properties for a high-purity Mg with 51 ppm Fe [31]. 5-sulfosalicylic acid has an inhibitory effect at low concentrations (linked to inhibition of iron redeposition) while, at high concentrations, it increases dissolution rate of Mg due to its ability to form soluble complexes with Mg^{2+} [32]. The mode of action of salicylates is therefore multiple and highly dependent on the experimental conditions, but most often associated with inhibition of iron redeposition.

This short review emphasizes that finding an inhibitor, that is efficient for a wide variety of Mg alloys (elemental composition and microstructure) and corrosive media (corrosive salt concentration and pH) and without risk of accelerating dissolution of Mg when its concentration is insufficient (as in the case of molybdate [28]) or too high (as in the case of 3,5-dinitrosalicylic acid on E21 alloy [2]), remains an important challenge.

The aim of this work is to gain a better understanding of the corrosion inhibition mechanisms of the WE43 Mg alloy by salicylate compounds. The study was focussed on two derivatives (salicylic acid (SA) and 3,5-dinitrosalicylic acid (DNSA)) in order to assess the influence of the nitro substitution in salicylic acid on the inhibition properties. To the best of our knowledge, no comprehensive studies have been carried out on the mechanism of action of salicylate inhibitors on the corrosion of rare-earth Mg alloys, such as the WE43 Mg alloy. Electrochemical measurements and inductive coupled plasma-optical emission spectrometry (ICP-OES) as well as continuous pH monitoring were performed after different immersion times in a 0.2 M NaCl solution. Scanning electron microscopy (SEM) and energy-dispersive X-ray spectroscopy (EDX) analyses were conducted to characterize the morphology and the composition of the corrosion product layers. The inhibition mechanism was finally discussed on the basis of the obtained results and in relation to the acid-base properties of the inhibitors and the thermodynamic equilibrium constants of the various oxides layers likely to be formed.

2. Experimental

2.1. Materials and reagents

The WE43 Mg alloy was supplied by Prodem-Bonnans. The nominal composition, provided by the supplier, is reported in Table 1 and is in accordance with ASTM B951–11. Fig. 1 shows a SEM micrograph of the alloy microstructure. As previously described [33], it consists in the α-Mg matrix, mainly enriched in Y, and the presence of various particles randomly distributed inside the matrix: cubic Y-rich particles and Nd-rich particles (Fig. 1). The micrograph also reveals whitish Zr-rich regions and a submicrometer acicular phase, identified by Coy et al. as β-$Mg_{14}Nd_2Y$ [34].

The two inhibitors: salicylic acid (SA) and 3,5-dinitro salicylic acid (DNSA) were purchased from Sigma-Aldrich and used as received. Their molecular structures are shown in Fig. 2. For each inhibitor, several concentrations were tested (50 μM, 500 μM, 5 mM and 10 mM). In the present work, only the results for the concentration which gave the best inhibition efficiency (5 mM for both SA and DNSA) were reported.

The corrosive medium was prepared from deionized water by adding 0.2 M NaCl (reagent grade). With the inhibitors, the pH of the solutions was adjusted with concentrated NaOH to reach a pH value of 6, corresponding to the natural pH of the NaCl blank solution. Both SA and DNSA were soluble in the 0.2 M NaCl solution without any addition of organic solvent. Their solubility limits, in water at 25°C, are 11 mM and 66 mM for SA and DNSA, respectively [35,36]. It can be emphasized that DNSA is totally ionized in water. Thus, adding NaOH to reach a pH of 6 does not alter its solubility. SA, on the other hand, is only partially ionized in water (46 % for 5 mM) due to a higher pKa (lower acidity) than DNSA. Its solubility therefore increases with its degree of ionization when NaOH is added to reach a pH of 6 [37].

2.2. Electrochemical measurements

Electrochemical measurements were carried out using a classical three-electrode cell. The working electrode was a rotating WE43 Mg disc electrode (RDE). The electrode was fabricated in the form of a cylinder with a surface area of 1 cm^2. The lateral part of the electrode was covered with a heat-skinkable sheath. The electrode was polished down to SiC P4000, rinsed with ethanol and dried with hot air prior to immersion. A saturated calomel electrode (SCE) served as reference electrode and a graphite electrode as counter electrode. The working electrode rotation rate was set at 250 rpm. The measurements were conducted at least in duplicate with a computer-controlled VSP-300-based multichannel system (Bio-Logic SA, France) with EC-Lab ® software. The electrochemical impedance measurements were carried out with a sinusoidal perturbation of 30 mV_{RMS} with 4 points per decade in the frequency range 65 kHz to 20 mHz for short immersion times (from

Table 1
Nominal composition (wt%) of the WE43 Mg alloy.

Y	Nd	Zr	Zn	Mn	Fe	HRE	TRE	ORE	Mg
4.2	2.2	0.49	0.01	0.01	0.002	0.88	3.1	-	Bal

Other Rare Earth (ORE) shall principally be La, Ce, Pr, Nd, Gd, Dy, Er, Yb
HRE Heavy Rare Earth, TRE Total Rare Earth

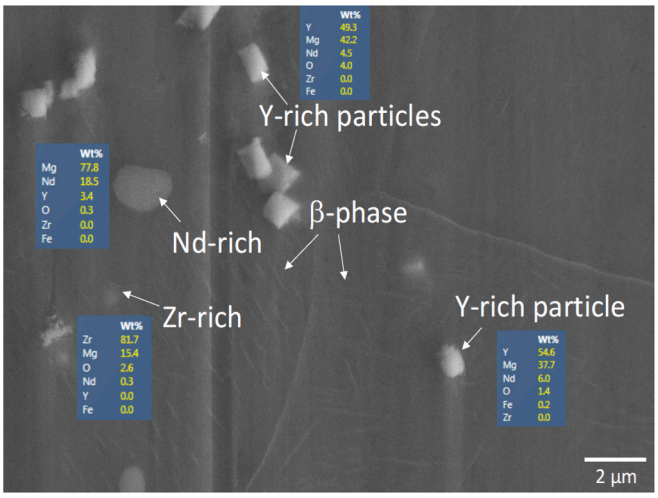

Fig. 1. SEM image of the WE43 Mg alloy (as-polished). The elemental composition obtained by EDX analysis of the particles indicated by the white arrows is also shown.

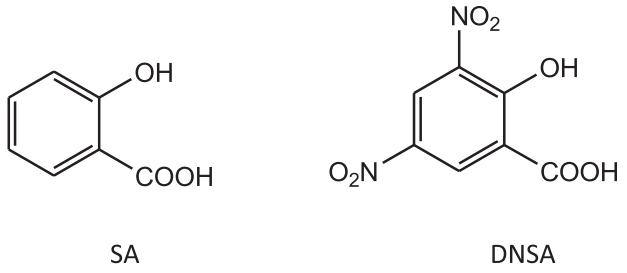

Fig. 2. Molecular structure of the two inhibitors: salicylic acid (SA) and 3,5 dinitro-salicylic acid (DNSA).

the beginning of immersion up to 1 h) and 8 points per decade from 65 kHz to 4 mHz for longer immersion times (from 1 h up to 24 h). The polarization curves were obtained from the cathodic range (-0.5 V below the open circuit potential (OCP)) to the anodic range (+0.5 V above the OCP) at scan rate of 20 mV min^{-1}. The polarization curves were corrected for ohmic drop by using the high-frequency impedance value as the electrolyte resistance.

2.3. pH measurements

The variation in pH of the solutions during the corrosion process was monitored continuously by using an Origalys OrigaMeter OpH218 with an Ag/AgCl pH electrode. The WE43 Mg RDE was immersed in 60 mL of the 0.2 M NaCl solution with and without the inhibitors.

2.4. ICP-MS analysis

Quantitative analyses of dissolved Mg in the electrolyte was conducted using a Perkin Elmer NexION 300X ICP-MS instrument. During the pH control experiment, 5 mL of the solution were taken after 2 h, 6 h and 24 h of immersion to determine the concentration of Mg^{2+} ions. A dilution factor of 10–50 was adopted depending on the sample concentration to enter the measurement range.

2.5. Characterization of the protective layers: morphology and composition

SEM images were obtained with a Zeiss Supra 40 VP/GEMINI Column equipped with an energy dispersive X-ray detector (EDX). SEM images and EDX spectra were collected at an accelerating voltage of 15 kV. Samples (20 mm×20 mm x 3 mm) used for SEM/EDX characterization were grounded with SiC papers and polished with diamond pastes (down to 1 µm). After the surface preparation, the samples were ultrasonically cleaned in ethanol and dried. Then, they were placed face up on the bottom of a beaker filled with a 0.2 M NaCl solution with or without inhibitor during various periods of time. The SEM/EDX analyses were performed on the top surface of the samples.

2.6. Job plot method

The method of Job was used to assess the possibility of molecular association (*i.e.* complexation) between magnesium ions and DNSA [38]. Job plots were carried out at two different pH (6 and 11) to cover the range of pH of the electrolyte during the corrosion test. Solutions of magnesium nitrate ($Mg(NO_3)_2.6H_2O$) and DNSA were prepared with an equal concentration of 1 mM. Various aliquots of these two mother solutions were mixed to obtain solutions with different Mg(II) concentrations (from 0 µM to 200 µM) completed with DNSA to obtain a total (Mg(II)+DNSA) concentration of 200 µM. The solutions were adjusted to the required pH value with 0.1 M NaOH or HCl. UV–visible spectra were recorded on a Shimadzu UV-1800 spectrophotometer.

3. Results and discussion

3.1. Electrochemical measurements

The variation of the OCP for the WE43 Mg alloy during immersion in the 0.2 M NaCl solution with and without SA and DNSA is shown in Fig. 3a. The modification in pH of the solution in the presence or absence of inhibitor is shown in Fig. 3b. Without inhibitor, the OCP increases during the first 2 h of immersion and then slightly decreases before stabilizing, after about 16 h, at a value of −1.95 V/SCE. The increase in potential, at the beginning of immersion, follows a rapid increase in pH up to a maximum value close to 10.6, in agreement with different works in the literature [39,40]. The initial increase of the OCP with time is generally attributed to the development of a film composed of MgO/$Mg(OH)_2$ on the sample surface [20,25,40].

In the presence of SA, the initial OCP values are slightly shifted to more negative values compared to the blank solution and then, it follows approximately the same variation to reach a stable value close to that obtained for the blank solution (-1.92 V/SCE). The addition of SA slightly decreases the pH in the first hours of immersion compared to the blank solution but the pH reaches values close to 10 after 3 h of immersion. In the presence of DNSA, the initial OCP value is significantly shifted to a more positive value (-1.65 V/SCE) and then, the OCP decreases up to −1.83 V/SCE during the first 2 h. Then, it shows a gradual increase throughout the test (24 h) up to a value of −1.79 V/SCE, which is about 160 mV more anodic compared to the blank solution. In the presence of DNSA, the pH gradually increases from 6.0 to 9.0 within 24 h. Thus, the release of hydroxide ions in the solution would be hindered in presence of DNSA.

Polarization curves obtained in the 0.2 M NaCl solution with and without SA and DNSA after 24 h of immersion at the OCP are shown in Fig. 4.

In the anodic domain, in the presence or absence of inhibitors, a pseudo-passive behaviour is observed followed by an inflexion point that is generally related to the breakdown of the protective film formed on the metal surface [33,41]. The anodic current densities in the presence of DNSA are lower compared to those obtained with SA or for the blank solution. Thus, DNSA has the characteristics of an anodic inhibitor. The difference between the breakdown potential, E_b, and the corrosion potential, E_{corr}, was calculated to compare the resistance to local breakdown of the surface films, formed after 24 h of immersion. This parameter is reported in Table 2. The (E_b-E_{corr}) difference is around 60 mV higher in the presence of SA or DNSA in the medium compared to

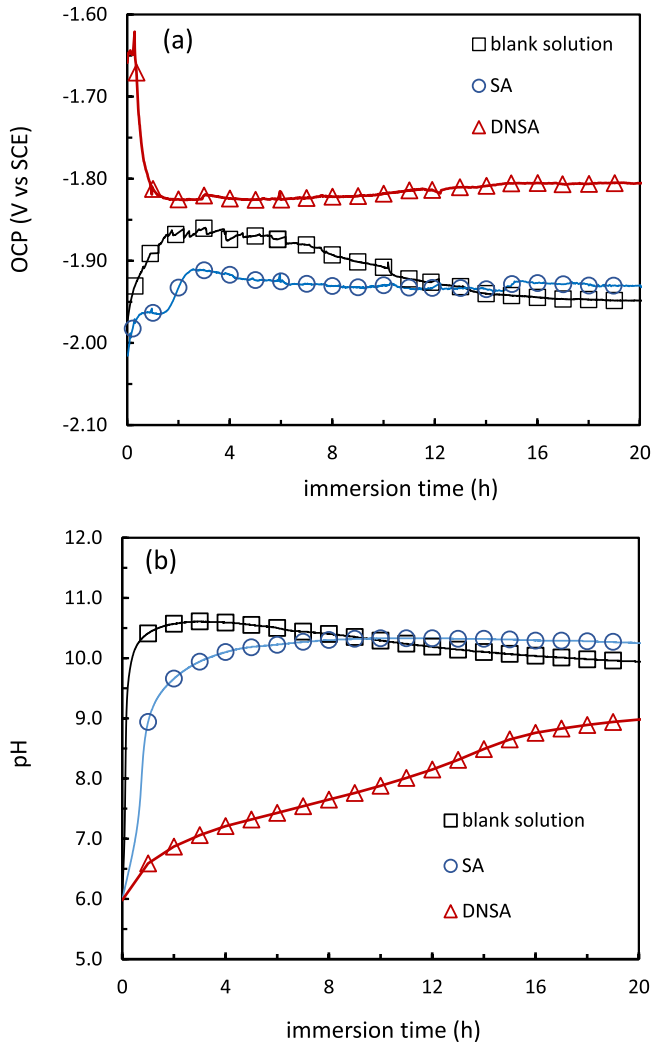

Fig. 3. Variation with immersion time of: (a) open circuit potential (OCP) for the WE43 Mg alloy with or without inhibitors and (b) pH of the 0.2 M NaCl solution with or without inhibitors.

the value in the blank NaCl solution. This might indicate that the addition of SA and DNSA in the electrolyte results in a modification of the oxide/hydroxide layer which would be more resistant to localized breakdown.

The instantaneous inhibitive efficiency, η, was graphically assessed from the cathodic branch of the polarisation curves, according to the following formula:

$$\eta(\%) = 100 \quad x \quad \frac{i_{corr(0)} - i_{corr}}{i_{corr(0)}} \qquad (1)$$

Where i_{corr} and $i_{corr(0)}$ are the corrosion current densities in the presence and absence of inhibitor, respectively. The values of the cathodic slopes, b_c, and of the instantaneous inhibitive efficiency, η, are reported in Table 2.

The cathodic curves are modified in the DNSA or in the SA-containing solutions by comparison with the blank NaCl solution. The instantaneous inhibitive efficiency, η, after 24 h of immersion is very low (6 %) in the presence of SA and reach a value of 40 % in the presence of DNSA.

Fig. 5 compares the impedance spectra obtained at the OCP for the WE43 Mg alloy for three immersion times with and without SA or DNSA in the NaCl solution. Regardless of the immersion time, the spectra show three time constants. The high frequency capacitive loop results from

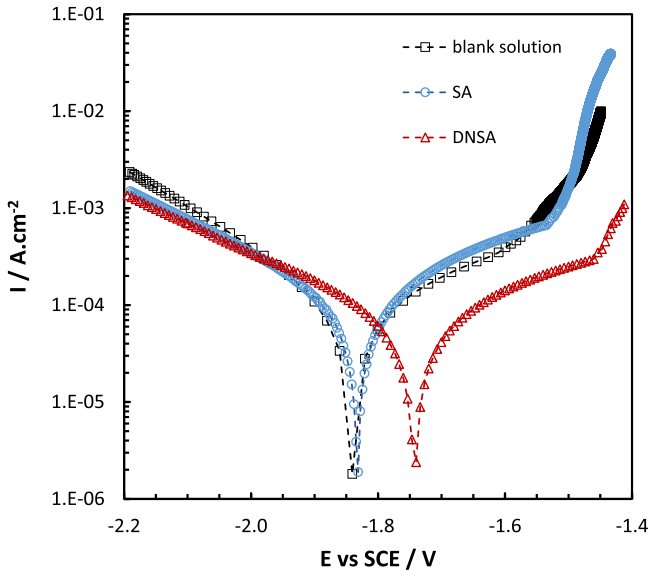

Fig. 4. Polarization curves obtained for the WE43 Mg alloy after 24 h of immersion in the 0.2 M NaCl solution (blank solution) and in the presence of the inhibitors.

Table 2
Parameter values graphically extracted from the polarisation curves for the WE43 Mg alloy after 24 h of immersion in a 0.2 M NaCl solution with and without the presence of inhibitors. Mean values of E_{corr} and E_b are given with standard deviation not exceeding 0.015 V.

Electrolytic solution	E_{corr} (V/ SCE)	E_b (V/ SCE)	E_b–E_{corr} (V/SCE)	-b_c (mV dec^{-1})	i_{corr} (μA cm^{-2})	η (%)
Blank	−1.84	−1.60	0.24	245 ± 10	96 ± 8	-
SA	−1.83	−1.53	0.30	290 ± 20	91 ± 5	~6
DNSA	−1.76	−1.45	0.31	320 ± 20	58 ± 5	~40

the charge transfer resistance, R_T and of the oxide film capacitance, C_f. The second time constant, at mid-frequencies, corresponds to the diffusion of Mg^{2+} ions through the porous oxide/hydroxide film and the inductive loop at low frequency would be related to relaxation process of adsorbed species, most likely $(Mg^{+})_{ads}$ [40,42,43]. The charge transfer resistance, R_T, was graphically determined from the diameter of the high-frequency capacitive loop [20]. The variation of R_T with immersion time is shown in Fig. 6.

Without inhibitor, the increase in the R_T values throughout 24 h immersion is attributed to the progressive formation of a surface film, probably MgO, which decreases the active surface area [33]. In the presence of SA and DNSA in the NaCl solution, the R_T values for short immersion times (< 2 h) are lower than those determined in the blank solution. The alloy surface therefore appears more active for short immersion times in the presence of SA and DNSA, which could be due to a delaying effect for the formation of the oxide/hydroxide film on the surface. This effect appears more pronounced with DNSA, notably at the beginning of immersion. In the SA-containing solution, this effect gradually diminishes, leading to a R_T value (390 Ω cm^2) slightly higher than that obtained for the blank solution after 24 h of immersion (350 Ω cm^2). In the presence of DNSA, the increase of R_T is significant when the immersion time increases. A R_T value of around 620 Ω cm^2 is reached after 24 h of immersion. This might account for the formation of a more protective film for longer immersion times, in agreement with the polarisation curves. It is also observed that in the presence of DNSA, the

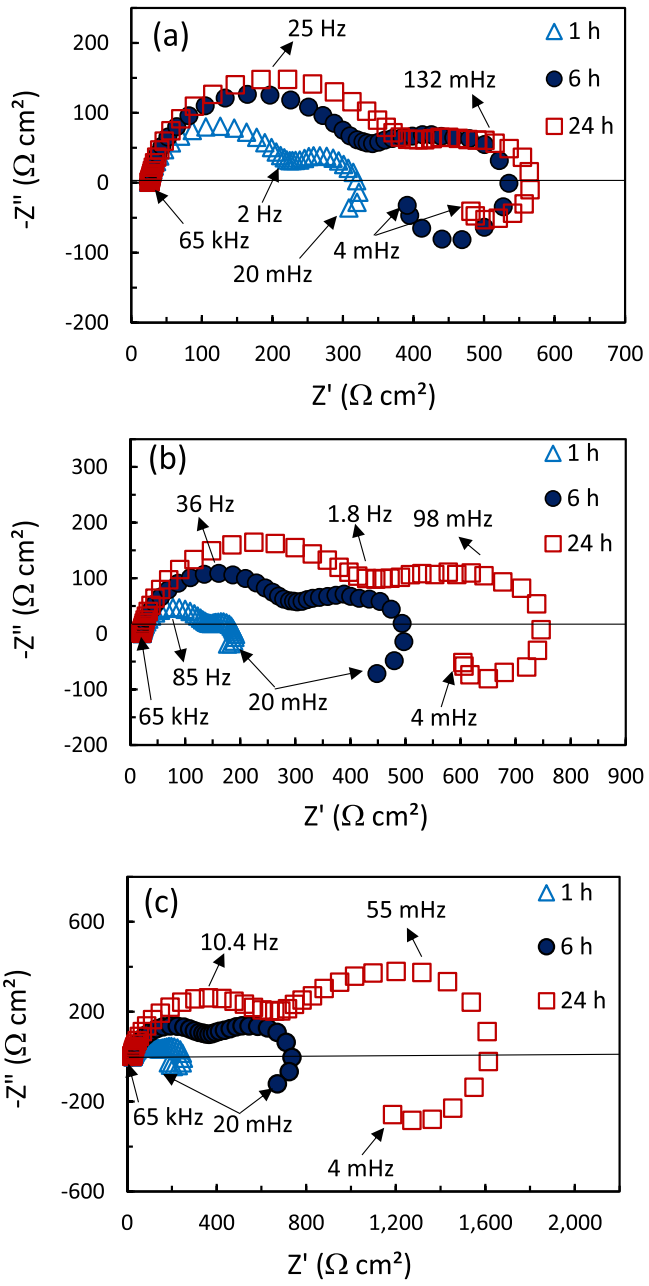

Fig. 5. Impedance spectra obtained for the WE43 Mg alloy after three different hold times in the 0.2 M NaCl solution: (a) without inhibitor and with the addition of inhibitor: (b) SA and (c) DNSA.

medium frequency and the inductive loops are more affected compared to those obtained in the presence of SA or for the blank solution (Fig. 5). The marked increase in the diameter of the medium frequency loop with DNSA suggests that the diffusion of Mg^{2+} through the corrosion products is slowed down.

The instantaneous inhibitive efficiency, η, was deduced from the EIS results according to the relationship:

$$\eta(\%) = 100 \times \frac{R_T - R_{T(0)}}{R_T} \quad (2)$$

where R_T and $R_{T(0)}$ are the charge transfer resistances in the presence and absence of inhibitor measured after 24 h immersion, respectively.

From the impedance results, SA and DNSA have an inhibitive efficiency of 10 % and of 44 %, respectively. A good agreement between the two methods (EIS and polarization curves) used to determine the instantaneous efficiencies is noteworthy.

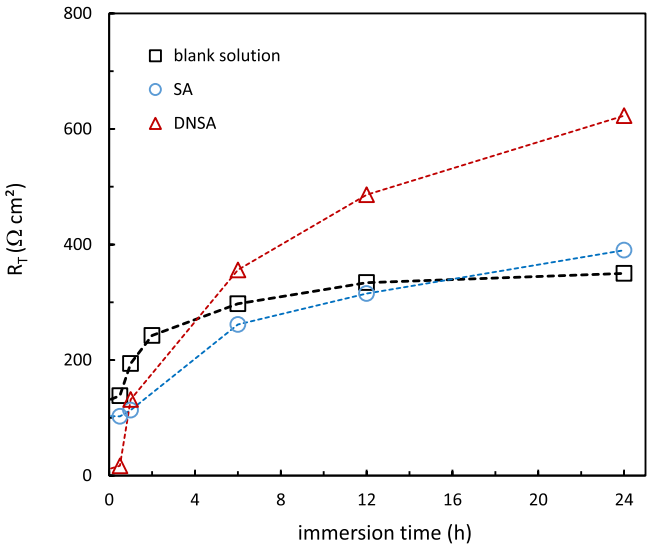

Fig. 6. Charge transfer resistance (R_T) versus immersion time in the 0.2 M NaCl solution: without inhibitor and with the addition of SA or DNSA.

Fig. 7 compares the mean corrosion rates (mm y^{-1}) calculated from the electrochemical data to those obtained from the ICP-OES measurements. Details of the expressions used to calculate the mean corrosion rates can be found elsewhere [20].

It can be seen that with and without inhibitor, the corrosion rate decreases when the immersion time increases. This again confirms the gradual deposition of corrosion products on the WE43 Mg alloy surface, even in the presence of the inhibitors.

The corrosion rates deduced from the electrochemical data are always lower than those determined from the ICP-OES analyses. This agrees with several works which have reported that electrochemical data underestimates the corrosion rate of Mg and Mg alloys [20,44–46]. It should be noted that using R_P, determined from an extrapolation on the X-axis at very low frequency, instead of R_T in the Stern-Geary relationship would lead to a greater difference between the two methods because, as can be seen in Fig. 5, R_P values are systematically higher than R_T values. Moreover, a value of n = 2 was used to calculate the

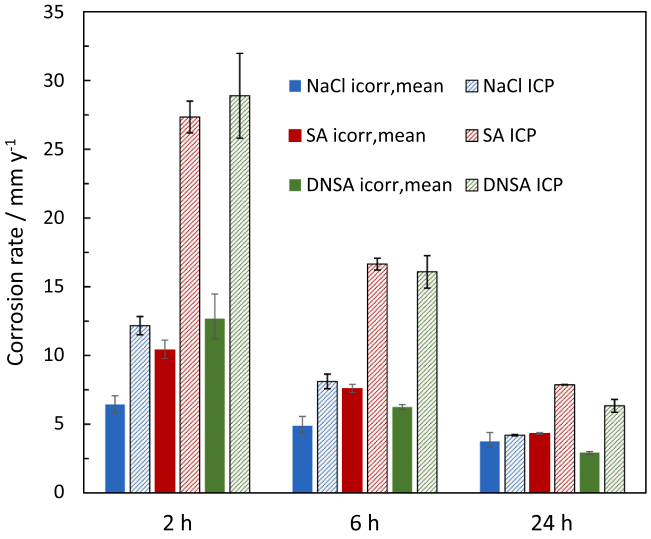

Fig. 7. Mean corrosion rates obtained from the ICP-OES measurements and from the electrochemical data [20] for the WE43 Mg alloy after 2 h, 6 h and 24 h of immersion in a 0.2 M NaCl solution with and without the presence of SA and DNSA (5 mM).

corrosion rate from the electrochemical data. It has been proposed that the corrosion rate determined from electrochemical data underestimates the actual corrosion rate due to a chemical reaction involving adsorbed intermediates, such as $(Mg^{+})_{ads}$. The hydrolysis of these adsorbed species generates H_2 and Mg^{2+} ions. Thus, the average number of electrons leading to the formation of one Mg^{2+} ion would be less than 2. Considering a value of $n < 2$ would lead to a better agreement between the corrosion rate determined from the electrochemical data and those calculated from the ICP-OES analysis. It is shown in Fig. 7 that the agreement between the two methods is better when the time range considered in the calculation increases. The average corrosion rate during 24 h immersion in the blank solution is close to that obtained in a 0.1 M Na_2SO_4 solution (between 4 and 5 mm y^{-1}) [20]. This is consistent with previous results which revealed no significant differences in electrochemical behaviour of the WE43 Mg alloy between chloride and sulfate media [33].

3.2. Surface morphology

The electrochemical results revealed that SA and DNSA have a substantial effect on the WE43 Mg alloy surface at the beginning of immersion. Thus, SEM observations were carried out with and without inhibitors, after very short immersion times and also after 24 h of immersion. Fig. 8 presents the SEM micrographs of the WE43 Mg alloy surface after 1 min and 5 min of immersion in the NaCl solution. For these short immersion times, hemispherical shape corrosion spots or domes are observed with a size ranging from a few μm up to 40 μm in diameter (Fig. 8a). Representative EDX spectra of the corrosion spots are shown in Fig. 8d. The O and Zr signals are more intense in the dome (spectrum 1) than away from the domes (spectrum 2). The high oxygen content suggests that the domes are mainly constituted of MgO/Mg $(OH)_2$ and the intense Zr signal would be consistent with the fact that the Zr-rich precipitates are the main cathodic sites [34]. Thus, H_2O reduction reaction over Zr-rich particles and clusters results in local alkalinisation and precipitation of $Mg(OH)_2$ around these particles. The formation of domes on rare earth Mg alloys has been reported by several authors [22,34,47].

Fig. 9 presents some SEM images of the WE43 Mg alloy surface after a short immersion time (< 5 min) in the NaCl solution with DNSA.

The morphology of the WE43 surface changes drastically in the presence of DNSA compared to that observed without inhibitor. Corrosion spots are virtually absent, replaced by filiform corrosion, clearly visible after a few minutes of immersion (Fig. 9a). Since these filiform deposits are not present after immersion in the blank solution, it is obvious that the presence of DNSA in the solution is responsible for their creation. From EDX analysis (Fig. 9d), it is seen that the O content in the thread is much more important than outside this area giving a O/Mg ratio close to 2, which agrees with a $Mg(OH)_2$ corrosion deposit. At higher magnification, the metal surface appears rather smooth, with fewer corrosion product deposits (Fig. 9c) than in the uninhibited solution (Fig. 8c).

SEM images of the WE43 Mg alloy surface after 24 h immersion with and without inhibitors are shown in Fig. 10.

For the blank solution, the surface appears heterogeneous and randomly distributed corrosion spots are still visible. At high magnification, the whole surface is covered by a corrosion product layer with a porous platelet-like structure (Fig. 10b). The surface films formed after 24 h immersion in the 0.2 M NaCl solution containing SA or DNSA show distinct morphologies compared to that observed in the blank solution. The films are more homogeneous and compact with a typical "mud-

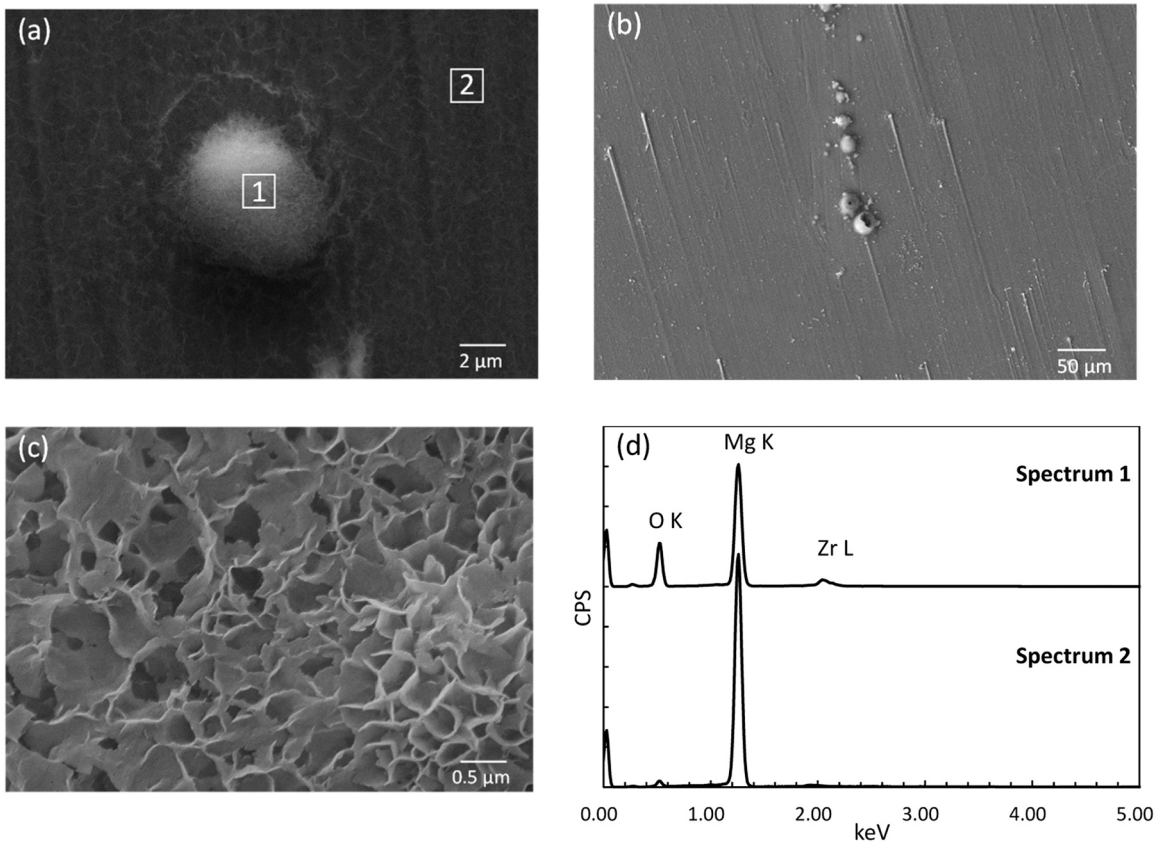

Fig. 8. SEM images of the WE43 Mg alloy surface in the blank solution (0.2 M NaCl): (a) after 1 min immersion to highlight a dome region; (b) after 5 min immersion at low magnification; (c) at high magnification to highlight the surface deposit morphology away from a dome; (d) EDX spectra obtained from selected regions referred as "1" and "2" in the SEM micrograph (a).

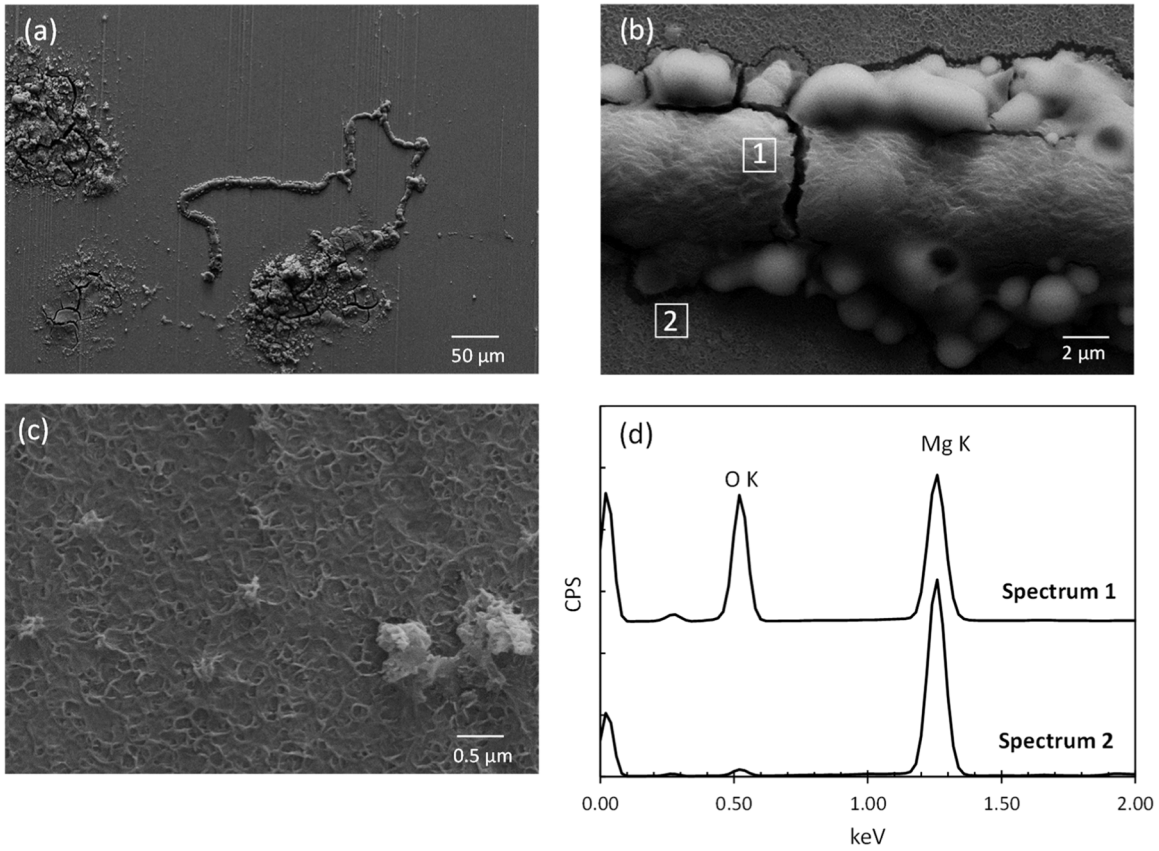

Fig. 9. SEM images of the WE43 alloy after 5 min immersion in 0.2 M NaCl-5 mM DNSA solution: (a) low magnification; (b) high magnification to highlight the morphology of a corrosion filament; (c) the surface deposit morphology away from a filament and (d) EDX spectra obtained from selected regions referred as "1" and "2" in the SEM micrograph (b).

cracking" appearance (Fig. 10c and e). Surface cracks might be due to dehydration of the films but it is noteworthy, that cracks were also observed by optical microscopy, showing that they did not occur after vacuum exposure during SEM analysis. From the SEM images at low magnification (Fig. 10c and e), there is apparently little difference in the morphology of the layer formed in the presence of SA or DNSA. However, at higher magnification (Fig. 10d and f), different film structures are visible. With SA, the surface film appears thick and rather porous with a morphology quite similar to that observed without inhibitor (Fig. 10b). In contrast, in the presence of DNSA, the surface film consists of a stack of plate-like grains of different sizes preferentially oriented parallel to the substrate (Fig. 10f).

EDX analyses were conducted at different locations on the surface (Table 3). Significant differences in the chemical composition of the films are observed.

EDX analyses of the corrosion deposit formed in the blank solution revealed the presence of O, Mg and of the alloying elements (Y, Nd and Zr). For the surfaces exposed to DNSA containing NaCl electrolyte, the presence of intense C and N signals indicates that DNSA is incorporated in a significant proportion into the corrosion products layer, probably in the form of complexes with the alloying elements of the WE43 Mg alloy. The intensity of the carbon signal is such that it cannot be associated with a simple adsorption of one molecular layer. The signal intensity of C is lower for the corrosion products formed in the SA containing electrolyte suggesting that this molecule is less likely to form insoluble complexes with the elements of the WE43 Mg alloy.

Fig. 11 compares Y/Mg, Nd/Mg and Zr/Mg ratios obtained from the EDX data both before and after immersion in the various electrolytes. In the presence of SA and DNSA in the electrolyte, the corrosion product layers are enriched in Y, Nd and Zr (probably in the form of Y_2O_3 or $Y(OH)_3$, of Nd_2O_3 and of ZrO_2) by comparison with the elemental composition of the WE43 Mg alloy before immersion. Moreover, this enrichment in alloying elements is significantly higher with DNSA.

In Fig. 12, the variation of O/Mg atomic ratio in the corrosion product layers as a function of the exposure time in the electrolyte with or without DNSA is reported.

In the blank solution, the O/Mg ratio increases rapidly during the first half-hour of immersion, then it stabilizes for longer immersion times. In contrast, when DNSA is present in the solution, the O/Mg ratio remains low during the first hour of immersion and steadily increases thereafter, reaching values well above 2 after 100 h of immersion. For short immersion times (30 min), in both the blank and DNSA solutions, the metal response contributes to the EDX signal. The increase in the O/Mg ratio suggests a thickening of the oxide layer over time, though this process occurs more slowly in the DNSA solution, indicating a potential inhibiting effect of the molecule. After 100 h of immersion, an O/Mg ratio of 2 suggests minimal substrate contribution to the EDX signal, implying a layer thickness in the micrometer range. Additionally, this indicates a significant contribution of rare-earth oxides and DNSA to the layer composition, in agreement with the results shown in Fig. 11 and Table 3.

3.3. *Corrosion inhibition mechanisms*

In the following, the origin of the greater inhibition efficiency of DNSA compared to SA is discussed on the basis of the experimental results. After a brief review of the corrosion mechanism of RE Mg alloys in aqueous media, the ability of SA and DNSA to (i) form soluble salts with Mg^{2+}, (ii) modify the interfacial pHs or (iii) the composition of the oxide layers and (iv) form insoluble organometallic complexes with the

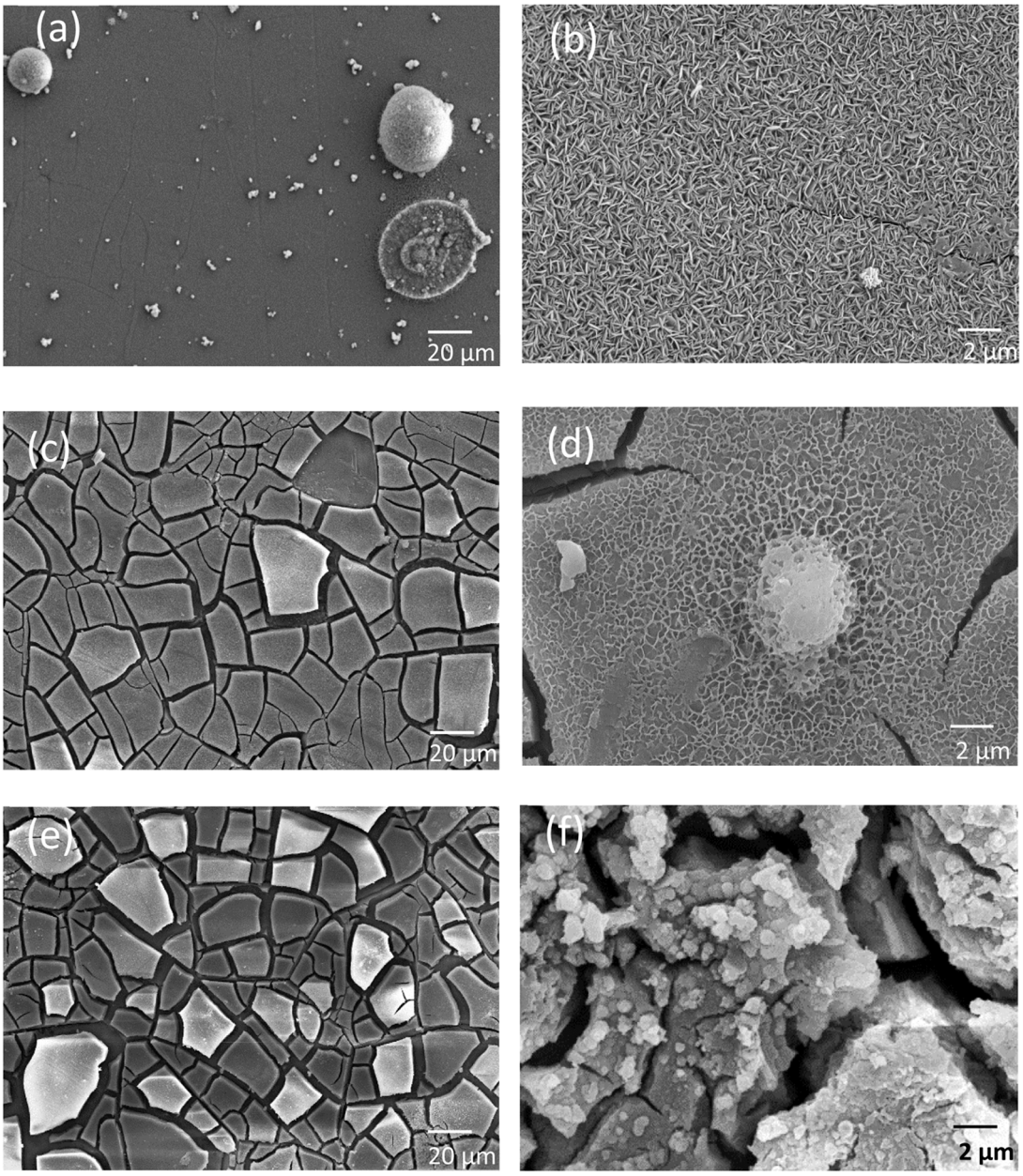

Fig. 10. SEM micrographs with two magnifications of the WE43 Mg alloy surface after 24 h immersion in: (a, b) 0.2 M NaCl, (c, d) 0.2 M NaCl + SA and (e, f) 0.2 M NaCl + DNSA.

Table 3
Elemental content in wt% obtained from EDX analysis on the WE43 Mg alloy surface before and after 24 h immersion.

Immersion condition	C	N	O	Mg	Y	Nd	Zr
No immersion	-	-	0.8 ±0.3	92.1 ±0.3	4.0 ±0.2	2.4 ±0.1	0.64 ±0.21
0.2 M NaCl	-	-	37±5	56.6 ±5.6	3.5 ±0.3	2.0 ±0.1	0.37 ±0.04
0.2 M NaCl-SA	16.6 ±0.6	-	26±4	49.6 ±5.6	4.5 ±0.5	2.7 ±0.3	0.67 ±0.08
0.2 M NaCl-DNSA	21.9 ±1.7	3.5 ±0.6	26±6	37.6 ±8.3	6.3 ±0.2	3.5 ±0.2	0.94 ±0.02

alloying elements, will be successively discussed.

The Mg corrosion mechanism is still being discussed, but the most commonly accepted reaction scheme is as follows [40,41,48–51]:

$$Mg \rightarrow Mg^{2+} + 2\,e^{-} \text{ (anodic dissolution of Mg)} \quad (3)$$

$$2\,H_2O + 2\,e^{-} \rightarrow 2\,OH^{-} + H_2 \text{ (cathodic hydrogen evolution)} \quad (4)$$

$$Mg^{2+} + 2\,OH^{-} \rightarrow Mg(OH)_2 \quad (5)$$

Then, a MgO layer is progressively formed according to the following equilibrium:

$$MgO + 2\,H_2O \leftrightarrow Mg(OH)_2 \quad (6)$$

For the WE43 Mg alloy, several authors have shown that the rare earths (Y and Nd) and Zr, present in solid solution in the Mg matrix, are also incorporated into the corrosion products layer formed on the surface. Their corrosion mechanisms would occur according to similar reaction schemes as for the Mg [24,27]:

$$Y \rightarrow Y^{3+} + 3\,e^{-} \quad (7)$$

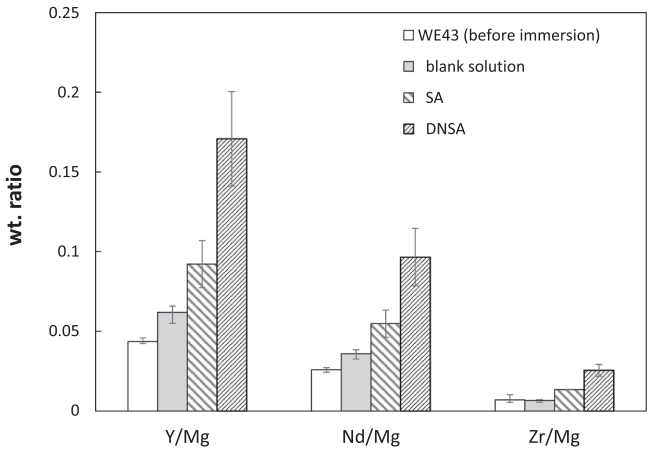

Fig. 11. Composition (Y, Nd, Zr / Mg (wt. ratio)) of the WE43 Mg alloy surface measured by EDX before and after 24 h immersion in 0.2 M NaCl; in 0.2 M NaCl + SA and in 0.2 M NaCl + DNSA.

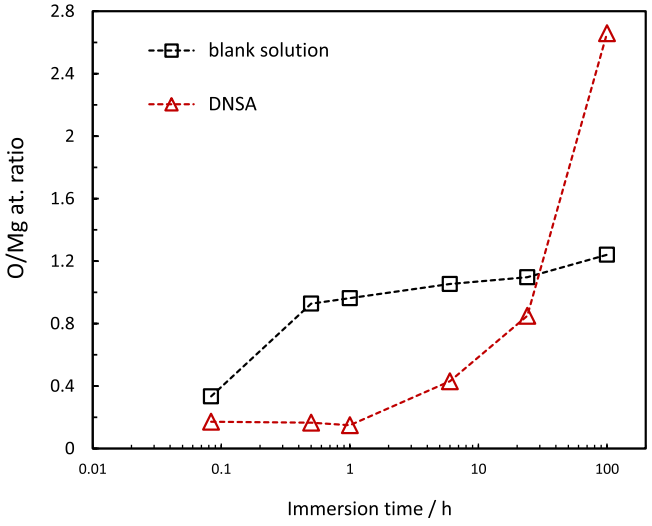

Fig. 12. O/Mg atomic ratio obtained from EDX analysis as a function of immersion time in a 0.2 M NaCl solution without and with DNSA.

$$Y^{3+} + 3\,OH^- \rightarrow Y(OH)_3 \quad (8)$$

$$Y_2O_3 + 3\,H_2O \leftrightarrow 2\,Y(OH)_3 \quad (9)$$

The reactions are only shown with Y as the same reaction schemes occur with Nd and Zr to lead to Nd_2O_3-$Nd(OH)_3$ and $Zr(OH)_4$-ZrO_2 deposits.

3.3.1. Complexation of SA derivatives with Mg^{2+}

In the blank solution and, in agreement with previous studies [22, 34], the most severe localised galvanic attack occurs at the adjacent areas of Zr-rich precipitates, as seen from SEM observations for short immersion times (Fig. 8). The situation is totally different with DNSA, for which filiform corrosion happens in the first moments of immersion (Fig. 9). This observation, in agreement with the initial significant shift of the OCP towards anodic values (Fig. 3a), suggests that DNSA interacts with the surface from the very beginning of immersion. First, it is noteworthy that the WE43 Mg alloy used in the present study contains only 20 ppm Fe which is a very low content to cause an acceleration of the corrosion rate. Thus, DNSA-Fe are unlikely to play a major role on the corrosion inhibition of the WE43 Mg alloy.

The Job method was used to investigate the possibility of complexation between Mg^{2+} ions and DNSA. The Job plots based on UV-Vis spectra gave a straight line with no curvature (Fig. 13). Therefore, unlike other salicylates (such as SA [52]), DNSA do not form complexes with Mg^{2+}, in agreement with the results found by Merce *et al.* [53]. This behaviour can be related to the withdrawing effect of the nitro groups which decrease the nucleophilicity of the phenolic substituent. The formation of soluble complexes between dissolved Mg^{2+} ions and DNSA cannot therefore explain the high rate of Mg dissolution observed at the beginning of immersion in the electrolyte.

3.3.2. Buffering effect of SA derivatives

The monitoring of the pH of the solution showed that DNSA considerably slowed down alkanisation of the medium while SA has no discernible effect compared to the blank solution (Fig. 3b). The acid-base properties of the two salicylic derivatives could be at the origin of this effect. First and second dissociation constants (pKa values) of 0.3 and 7.2 (at I = 0.2 M and T = 25°C) have been previously reported for DNSA (H_2L) [54]. For SA, the corresponding values are 2.7 and 13.4 [54]. The lower value of the first dissociation constant for DNSA compared to SA (*i.e.* increased acidity of the carboxyl group) results from the electron-withdrawing inductive effect of the nitro groups. The lower value of the second dissociation constant (phenol group) results from the electron-withdrawing resonant effect of the nitro groups. From these pKa values, it appears that SA and DNSA are dissociated in ionic form under the initial conditions (pH = 6). Unlike SA, DNSA can deprotonate by trapping OH^- ions from water reduction (reaction (10)) thus, slowing the pH rise at the metal/solution interface. This could hinder the formation of $Mg(OH)_2$ at the surface, and explain the high initial Mg dissolution with DNSA (Fig. 6 and Fig. 7).

$$HL^- + OH^- \rightarrow L^{2-} + H_2O \quad (10)$$

Apart from the above buffering effect, the adsorption of DNSA on the surface of the $Mg(OH)_2$ embryos could also slow down the initial growth of $Mg(OH)_2$ crystals. Further experimental work would be required to investigate the kinetics of $Mg(OH)_2$ growth [17,29].

3.3.3. Enrichment of the corrosion products layers by the alloying elements (Y, Nd)

The increase in the charge transfer resistance (R_T) with immersion time (Fig. 5 and Fig. 6) was associated with the formation of the oxides film on the WE43 Mg surface. It is therefore expected that behaviour in the event of prolonged immersion will be dominated by the protective properties of this layer. EDX analyses showed a marked enrichment in Y and Nd of the films deposited on the surface with the two inhibitors, with a much higher enrichment with DNSA (Fig. 11). This rare-earth enrichment of the corrosion deposits usually leads to more protective films, notably due to a higher Pilling-Bedworth (PB) ratio for rare-earth

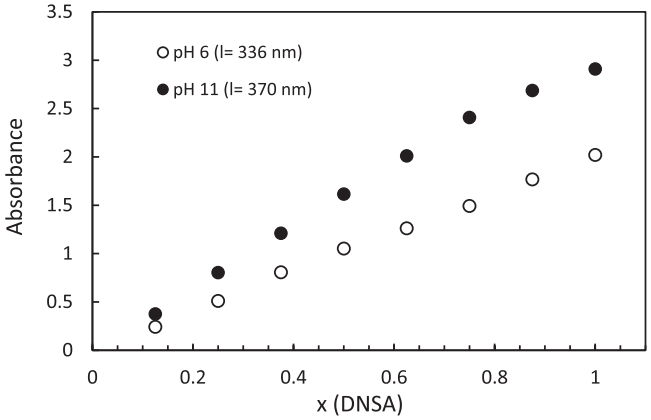

Fig. 13. Job diagram for DNSA and $Mg(NO_3)_2$ at pH = 6 and pH = 11 (x (DNSA) = mole fraction of DNSA).

oxides (PB ratio of 1.13 [55] or 1.39 [56] for Y oxides) compared to the PB ratio for MgO (0.8 [57]). The progressive Y and Nd enrichment with DNSA for long immersion times would be responsible for the increase in R_T values observed with DNSA (Fig. 6). The solubility products of Y $(OH)_3$ (K_{sp}~10^{-28}) and $Nd(OH)_3$ (K_{sp}~10^{-23}) [67] are lower than that of $Mg(OH)_2$ (K_{sp}~10^{-11}). Consequently, the pH values required for the onset of precipitation of $Y(OH)_3$ and $Nd(OH)_3$ are lower than in the case of $Mg(OH)_2$. As discussed in Section 3.3.2, DNSA buffered the bulk pH of the electrolyte at a value around pH = 9 after one day of immersion. However, it is likely that pH values allowing the deposit of $Mg(OH)_2$ was reached at the metal/electrolyte interface (approx. 9.5 for a Mg^{2+} concentration of 10^{-2} M). The buffering effect of DNSA does not, of course, inhibits $Mg(OH)_2$ formation, but it enables greater enrichment of Y and Nd than that observed for the blank NaCl solution.

3.3.4. Formation of insoluble SA and DNSA complexes with the alloying elements

SEM/EDX surface analysis showed that DNSA and SA are incorporated into the oxide layer (Table 3), suggesting the formation of complexes with the rare-earth elements. 1:1 complexes of salicylic acid derivatives with Y(III) (Log K_1=8.61 for SA, Log K_1=5.82 for DNSA) and Nd(III) (Log K_1=8.15 for SA, Log K_1=5.39 for DNSA) metal ions have been reported [58,59]. The reactions of the formation of Y(III) and Nd (III) complexes can be written as:

$$Y^{3+} + HL^{-} \leftrightarrow [Y(III)L]^{+} + H^{+} \quad (11)$$

$$Nd^{3+} + HL^{-} \leftrightarrow [Nd(III)L]^{+} + H^{+} \quad (12)$$

Propensity of Y (III) and Nd (III) to form hydroxo species in aqueous solution [60] results in hydrolysis of the complexes at near-neutral conditions, according to reactions (13) and (14):

$$[Y(III)L]^{+} + H_2O \leftrightarrow [Y(III)(OH)L] + H^{+} \quad (13)$$

$$[Nd(III)L]^{+} + H_2O \leftrightarrow [Nd(III)(OH)L] + H^{+} \quad (14)$$

The stability constants of the hydroxometal-ligand complexes are relatively high (Log $K_{Y^{3+}}$ =7.69 and Log $K_{Nd^{3+}}$ =7.87 for SA and Log $K_{Y^{3+}}$ =7.16 and Log $K_{Nd^{3+}}$ =7.37 for DNSA [59]). It has been reported that the formation of the neutral hydroxometal-ligand complexes was accompanied by opacity/turbidity during potentiometric titration [59]. These complexes are therefore very slightly soluble in water and can be incorporated into the corrosion products formed on the WE43 Mg alloy surface. An inhibition mechanism based on the formation of DNSA-Y (Nd) precipitates filling the pores of the oxide deposits is supported by both the polarisation curves and the EIS results. The chelating and precipitation of DNSA with Y (Nd) require Y^{3+} (Nd^{3+}) ions which mainly come from anodic sites. The precipitation would therefore be greater under anodic polarization than under cathodic polarization, as seen in Fig. 4. This mechanism is also supported by the EIS results (Fig. 5). The deposited layer progressively hinders the diffusion of Mg^{2+}, as reflected by the gradual increase in the diameter of the mid frequency loop on the impedance diagrams. It is also worth noting that reactions (11–14) contribute, in addition to reaction (10), to limit the alkalinisation that accompanies the water cathodic reduction.

Addition of SA demonstrates an acceleration of the Mg dissolution for short immersion times and a corrosion rate of the same order of magnitude as that observed in the blank NaCl solution for long immersion times. This is because SA, unlike DNSA, forms stable complexes with Mg^{2+}, Log K_1=5.56 [61]. These soluble complexes can accelerate Mg dissolution which offsets the beneficial effect associated with the formation of Y and Nd complexes. As already noted, second deprotonation of SA cannot occur in the NaCl solution through reaction (10). This leads to a lower Y (and Nd) enrichment than with DNSA and, consequently, a lower protective deposit. It is noteworthy that SA has shown an inhibiting efficiency of 90 % for CP-Mg with a high content of Fe impurity (220 ppm) [62]. The inhibition performance was related to prevention of iron redeposition on Mg surface. In the present study, this mechanism is clearly not operative due to the low iron content of the WE43 alloy (20 ppm).

4. Conclusions

The corrosion inhibition of the WE43 Mg alloy by SA and DNSA was studied in a NaCl solution. Electrochemical measurements revealed different modes of action for the two compounds, confirmed by SEM and EDX analyses which showed that the morphologies and compositions of the corrosion product layers differed between the two inhibitors. Inhibitory properties were observed for DNSA for long immersion times (> 12 h), while SA did not show inhibitive effect.

The main characteristics of DNSA are as follows:

- it does not form complexes with Mg^{2+}
- it forms sparingly soluble hydroxo-complexes with Y^{3+} and Nd^{3+}
- it buffers the solution at near neutral pHs which allows the contribution of Y and Nd oxides to the deposited layer to be increased.

The formation of the protective layer is a slow process, lasting for some hours, because DNSA does not interact with the α-Mg matrix but only with the alloying elements (Y and Nd) and under pH conditions of Mg dissolution. Therefore, the Y and Nd enrichment of the corrosion products layer, in the form of oxides/hydroxides and hydroxo-complexes with DNSA, is gradual. In these processes, the acidic properties of DNSA, by buffering the interfacial pH, play a key role in explaining Y and Nd enrichments.

The results presented here showed that well-balanced acid-base properties of an inhibitor can have a beneficial effect on the corrosion inhibition properties of rare-earth Mg alloys in NaCl solutions. Results of this study can provide new directions for the development of effective corrosion inhibitors for rare-earth Mg alloys.

CRediT authorship contribution statement

Nadja Leibl: Writing – review & editing, Investigation. **François-Xavier Perrin:** Writing – review & editing, Writing – original draft, Validation, Supervision, Funding acquisition, Conceptualization. **Armand Fahs:** Writing – review & editing, Validation. **Lénaïk Belec:** Writing – review & editing, Validation. **Nicolas Caussé:** Writing – review & editing, Validation. **Nadine Pébère:** Writing – review & editing, Validation, Supervision.

Declaration of Competing Interest

The authors declare the following financial interests/personal relationships which may be considered as potential competing interests: Leibl Nadja reports financial support was provided by French National Research Agency. If there are other authors, they declare that they have no known competing financial interests or personal relationships that could have appeared to influence the work reported in this paper

Acknowledgements

This research was carried out with the technical and financial supports of the Direction Générale de l'Armement (DGA - France) under grant number ANR-18-ASTR-0016-01.

Data availability

Data will be made available on request.

References

[1] K. Gusieva, C.H.J. Davies, J.R. Scully, N. Birbilis, Corrosion of magnesium alloys: the role of alloying, Int. Mater. Rev. 60 (2015) 169–194, https://doi.org/10.1179/1743280414Y.0000000046.

[2] S.V. Lamaka, B. Vaghefinazari, D. Mei, R.P. Petrauskas, D. Höche, M. L. Zheludkevich, Comprehensive screening of Mg corrosion inhibitors, Corros. Sci. 128 (2017) 224–240, https://doi.org/10.1016/j.corsci.2017.07.011.

[3] A.F. Galio, S.V. Lamaka, M.L. Zheludkevich, L.F.P. Dick, I.L. Mueller, M.G. S. Ferreira, Inhibitor-doped sol-gel coatings for corrosion protection of magnesium alloy AZ31, Surf. Coat. Technol. 204 (2010) 1479–1486, https://doi.org/10.1016/j.surfcoat.2009.09.067.

[4] Y. Chen, X. Lu, S.V. Lamaka, P. Ju, C. Blawert, T. Zhang, F. Wang, M. L. Zheludkevich, Active protection of Mg alloy by composite PEO coating loaded with corrosion inhibitors, Appl. Surf. Sci. 504 (2020) 144462, https://doi.org/10.1016/j.apsusc.2019.144462.

[5] W. Jin, G. Wu, H. Feng, W. Wang, X. Zhang, P.K. Chu, Improvement of corrosion resistance and biocompatibility of rare-earth WE43 magnesium alloy by neodymium self-ion implantation, Corros. Sci. 94 (2015) 142–155, https://doi.org/10.1016/j.corsci.2015.01.049.

[6] B. Vaghefinazari, E. Wierzbicka, P. Visser, R. Posner, R. Arrabal, E. Matykina, M. Mohedano, C. Blawert, M.L. Zheludkevich, S.V. Lamaka, Chromate-free corrosion protection strategies for magnesium alloys—a review: Part III—corrosion inhibitors and combining them with other protection strategies, Materials 15 (2022) 8489, https://doi.org/10.3390/ma15238489.

[7] J.-L. Wang, C. Ke, K. Pohl, N. Birbilis, X.-B. Chen, The unexpected role of benzotriazole in mitigating magnesium alloy corrosion: a nucleating agent for crystalline nanostructured magnesium hydroxide film, J. Electrochem. Soc. 162 (2015) C403–C411, https://doi.org/10.1149/2.0781508jes.

[8] Z. Feng, B. Hurley, J. Li, R. Buchheit, Corrosion inhibition study of aqueous vanadate on Mg alloy AZ31, J. Electrochem. Soc. 165 (2018) C94, https://doi.org/10.1149/2.1171802jes.

[9] G. Williams, H.N. McMurray, R. Grace, Inhibition of magnesium localised corrosion in chloride containing electrolyte, Electrochim. Acta 55 (2010) 7824–7833, https://doi.org/10.1016/j.electacta.2010.03.023.

[10] A.A. Chirkunov, M.L. Zheludkevich, Corrosion inhibition of elektron WE43 magnesium alloy in NaCl solution, Int. J. Corros. Scale Inhib. 7 (2018). ⟨https://ijcsi.pro/papers/corrosion-inhibition-of-elektron-we43-magnesium-alloy-in-nacl-solution/⟩ (accessed June 27, 2023).

[11] N. Dinodi, A.N. Shetty, Alkyl carboxylates as efficient and green inhibitors of magnesium alloy ZE41 corrosion in aqueous salt solution, Corros. Sci. 85 (2014) 411–427, https://doi.org/10.1016/j.corsci.2014.04.052.

[12] J. Hu, D. Zeng, Z. Zhang, T. Shi, G.-L. Song, X. Guo, 2-Hydroxy-4-methoxy-acetophenone as an environment-friendly corrosion inhibitor for AZ91D magnesium alloy, Corros. Sci. 74 (2013) 35–43, https://doi.org/10.1016/j.corsci.2013.04.005.

[13] J. Hu, D. Huang, G. Zhang, G.-L. Song, X. Guo, Research on the inhibition mechanism of tetraphenylporphyrin on AZ91D magnesium alloy, Corros. Sci. 63 (2012) 367–378, https://doi.org/10.1016/j.corsci.2012.06.021.

[14] I.A. Kartsonakis, S.G. Stanciu, A.A. Matei, E.K. Karaxi, R. Hristu, A. Karantonis, C. A. Charitidis, Evaluation of the protective ability of typical corrosion inhibitors for magnesium alloys towards the Mg ZK30 variant, Corros. Sci. 100 (2015) 194–208, https://doi.org/10.1016/j.corsci.2015.07.028.

[15] X. Lu, Y. Li, P. Ju, Y. Chen, J. Yang, K. Qian, T. Zhang, F. Wang, Unveiling the inhibition mechanism of an effective inhibitor for AZ91 Mg alloy, Corros. Sci. 148 (2019) 264–271, https://doi.org/10.1016/j.corsci.2018.12.025.

[16] J. Chen, J. He, L. Li, Spectroscopic insight into the role of SDBS on the interface evolution of Mg in NaCl corrosive medium, Corros. Sci. 182 (2021) 109215, https://doi.org/10.1016/j.corsci.2020.109215.

[17] Y. Cui, T. Zhang, F. Wang, New understanding on the mechanism of organic inhibitors for magnesium alloy, Corros. Sci. 198 (2022) 110118, https://doi.org/10.1016/j.corsci.2022.110118.

[18] F. Czerwinski, Controlling the ignition and flammability of magnesium for aerospace applications, Corros. Sci. 86 (2014) 1–16, https://doi.org/10.1016/j.corsci.2014.04.047.

[19] C. Liu, S. Lu, Y. Fu, H. Zhang, Flammability and the oxidation kinetics of the magnesium alloys AZ31, WE43, and ZE10, Corros. Sci. 100 (2015) 177–185, https://doi.org/10.1016/j.corsci.2015.07.020.

[20] S. Leleu, B. Rives, N. Causse, N. Pébère, Corrosion rate determination of rare-earth Mg alloys in a Na2SO4 solution by electrochemical measurements and inductive coupled plasma-optical emission spectroscopy, J. Magnes. Alloy. 7 (2019) 47–57, https://doi.org/10.1016/j.jma.2018.12.002.

[21] R. Arrabal, E. Matykina, F. Viejo, P. Skeldon, G.E. Thompson, Corrosion resistance of WE43 and AZ91D magnesium alloys with phosphate PEO coatings, Corros. Sci. 50 (2008) 1744–1752, https://doi.org/10.1016/j.corsci.2008.03.002.

[22] P.-W. Chu, E.A. Marquis, Linking the microstructure of a heat-treated WE43 Mg alloy with its corrosion behavior, Corros. Sci. 101 (2015) 94–104, https://doi.org/10.1016/j.corsci.2015.09.005.

[23] B. Feng, G. Liu, P. Yang, S. Huang, D. Qi, P. Chen, C. Wang, J. Du, S. Zhang, J. Liu, Different role of second phase in the micro-galvanic corrosion of WE43 Mg alloy in NaCl and Na2SO4 solution, J. Magnes. Alloy. 10 (2022) 1598–1608, https://doi.org/10.1016/j.jma.2020.12.013.

[24] H. Ardelean, A. Seyeux, S. Zanna, F. Prima, I. Frateur, P. Marcus, Corrosion processes of Mg–Y–Nd–Zr alloys in Na2SO4 electrolyte, Corros. Sci. 73 (2013) 196–207, https://doi.org/10.1016/j.corsci.2013.03.036.

[25] R. Arrabal, E. Matykina, F. Viejo, P. Skeldon, G.E. Thompson, Corrosion resistance of WE43 and AZ91D magnesium alloys with phosphate PEO coatings, Corros. Sci. 50 (2008) 1744–1752, https://doi.org/10.1016/j.corsci.2008.03.002.

[26] F. Zucchi, V. Grassi, A. Frignani, C. Monticelli, G. Trabanelli, Influence of a silane treatment on the corrosion resistance of a WE43 magnesium alloy, Surf. Coat. Technol. 200 (2006) 4136–4143, https://doi.org/10.1016/j.surfcoat.2005.02.073.

[27] L.M. Calado, M.G. Taryba, Y. Morozov, M.J. Carmezim, M.F. Montemor, Cerium phosphate-based inhibitor for smart corrosion protection of WE43 magnesium alloy, Electrochim. Acta 365 (2021) 137368, https://doi.org/10.1016/j.electacta.2020.137368.

[28] D.S. Kharitonov, M. Zimowska, J. Ryl, A. Zieliński, M.A. Osipenko, J. Adamiec, A. Wrzesińska, P.M. Claesson, I.I. Kurilo, Aqueous molybdate provides effective corrosion inhibition of WE43 magnesium alloy in sodium chloride solutions, Corros. Sci. 190 (2021) 109664, https://doi.org/10.1016/j.corsci.2021.109664.

[29] A. Maltseva, S.V. Lamaka, K.A. Yasakau, D. Mei, D. Kurchavov, M.L. Zheludkevich, G. Lefèvre, P. Volovitch, In situ surface film evolution during Mg aqueous corrosion in presence of selected carboxylates, Corros. Sci. 171 (2020) 108484, https://doi.org/10.1016/j.corsci.2020.108484.

[30] L. Fockaert, T. Wuerger, R. Unbehau, B. Boelen, R.H. Meissner, S. Lamaka, M. L. Zheludkevich, H. Terryn, J.M.C. Mol, ATR-FTIR in Kretschmann configuration integrated with electrochemical cell as in situ interfacial sensitive tool to study corrosion inhibitors for magnesium substrates, Electrochim. Acta 345 (2020) 136166, https://doi.org/10.1016/j.electacta.2020.136166.

[31] K.A. Yasakau, A. Maltseva, S.V. Lamaka, D. Mei, H. Orvi, P. Volovitch, M.G. S. Ferreira, M.L. Zheludkevich, The effect of carboxylate compounds on Volta potential and corrosion inhibition of Mg containing different levels of iron, Corros. Sci. 194 (2022) 109937, https://doi.org/10.1016/j.corsci.2021.109937.

[32] Y. Zhou, X. Lu, M.L. Zheludkevich, F. Wang, Tailoring corrosion and discharge performance of Mg anode by corrosion inhibitor, Electrochim. Acta 436 (2022) 141471, https://doi.org/10.1016/j.electacta.2022.141471.

[33] S. Leleu, B. Rives, J. Bour, N. Causse, N. Pébère, On the stability of the oxides film formed on a magnesium alloy containing rare-earth elements, Electrochim. Acta 290 (2018) 586–594, https://doi.org/10.1016/j.electacta.2018.08.093.

[34] A.E. Coy, F. Viejo, P. Skeldon, G.E. Thompson, Susceptibility of rare-earth-magnesium alloys to micro-galvanic corrosion, Corros. Sci. 52 (2010) 3896–3906, https://doi.org/10.1016/j.corsci.2010.08.006.

[35] F.L. Nordström, Å.C. Rasmuson, Solubility and melting properties of salicylic acid, J. Chem. Eng. Data 51 (2006) 1668–1671, https://doi.org/10.1021/je060134d.

[36] X. Zhao, G. Han, H. Zhao, Solubility of 3,5-dinitrosalicylic acid in fourteen pure solvents over temperatures from 278.15 to 323.15 K, J. Chem. Eng. Data 65 (2020) 2230–2237, https://doi.org/10.1021/acs.jced.0c00122.

[37] D.P. Otto, J. Combrinck, A. Otto, L.R. Tiedt, M.M. De Villiers, Dissipative particle dynamics investigation of the transport of salicylic acid through a simulated in vitro skin permeation model, Pharmaceuticals 11 (2018) 134, https://doi.org/10.3390/ph11040134.

[38] P. Job, Formation and stability of inoganic complexes in solution, Ann. De. Chim. 10 (1928) 113–203.

[39] N. Pebere, C. Riera, F. Dabosi, Investigation of magnesium corrosion in aerated sodium sulfate solution by electrochemical impedance spectroscopy, Electrochim. Acta 35 (1990) 555–561, https://doi.org/10.1016/0013-4686(90)87043-2.

[40] G. Baril, G. Galicia, C. Deslouis, N. Pébère, B. Tribollet, V. Vivier, An impedance investigation of the mechanism of pure magnesium corrosion in sodium sulfate solutions, J. Electrochem. Soc. 154 (2007) C108–C113, https://doi.org/10.1149/1.2401056.

[41] G.-L. Song, K.A. Unocic, The anodic surface film and hydrogen evolution on Mg, Corros. Sci. 98 (2015) 758–765, https://doi.org/10.1016/j.corsci.2015.05.047.

[42] M. Ascencio, M. Pekguleryuz, S. Omanovic, An investigation of the corrosion mechanisms of WE43 Mg alloy in a modified simulated body fluid solution: The influence of immersion time, Corros. Sci. 87 (2014) 489–503, https://doi.org/10.1016/j.corsci.2014.07.015.

[43] A.Z. Benbouzid, M.P. Gomes, I. Costa, O. Gharbi, N. Pébère, J.L. Rossi, M.T.T. Tran, B. Tribollet, M. Turmine, V. Vivier, A new look on the corrosion mechanism of magnesium: an EIS investigation at different pH, Corros. Sci. 205 (2022) 110463, https://doi.org/10.1016/j.corsci.2022.110463.

[44] Z. Qiao, Z. Shi, N. Hort, N.I. Zainal Abidin, A. Atrens, Corrosion behaviour of a nominally high purity Mg ingot produced by permanent mould direct chill casting, Corros. Sci. 61 (2012) 185–207, https://doi.org/10.1016/j.corsci.2012.04.030.

[45] A. Pardo, S. Feliu, M. Merino, R. Arrabal, E. Matykina, Electrochemical estimation of the corrosion rate of magnesium/aluminium alloys, Int. J. Corros. 2010 (2010), https://doi.org/10.1155/2010/953850.

[46] G. Song, A. Atrens, Corrosion of non-ferrous alloys. III. magnesium alloys, Mater. Sci. Technol. (2013), https://doi.org/10.1002/9783527603978.mst0406.

[47] R.M. Asmussen, W.J. Binns, P. Jakupi, D. Shoesmith, The Influence of microstructure on the corrosion of magnesium alloy ZEK100, Corrosion 71 (2014) 242–254, https://doi.org/10.5006/1387.

[48] M.P. Brady, G. Rother, L.M. Anovitz, K.C. Littrell, K.A. Unocic, H.H. Elsentriecy, G.-L. Song, J.K. Thomson, N.C. Gallego, B. Davis, Film breakdown and nano-porous Mg(OH)2 formation from corrosion of magnesium alloys in salt solutions, J. Electrochem. Soc. 162 (2015) C140, https://doi.org/10.1149/2.0171504jes.

[49] A. Atrens, G.-L. Song, M. Liu, Z. Shi, F. Cao, M.S. Dargusch, Review of recent developments in the field of magnesium corrosion, Adv. Eng. Mater. 17 (2015) 400–453, https://doi.org/10.1002/adem.201400434.

[50] G.L. Song, A. Atrens, Corrosion mechanisms of magnesium alloys, Adv. Eng. Mater. 1 (1999) 11–33, https://doi.org/10.1002/(SICI)1527-2648(199909)1:1<11::AID-ADEM11>3.0.CO;2-N.

[51] S. Thomas, N.V. Medhekar, G.S. Frankel, N. Birbilis, Corrosion mechanism and hydrogen evolution on Mg, Curr. Opin. Solid State Mater. Sci. 19 (2015) 85–94, https://doi.org/10.1016/j.cossms.2014.09.005.
[52] N.A. Lange. Lange's Handbook Of Chemistry, 15. ed, McGraw-Hill, New York, NY, 1999.
[53] A.L.R. Mercê, A.S. Mangrich, B. Szpoganicz, N.M. Levy, J. Felcman, Potentiometric equilibrium constants for complexes of nitrosalicylic acids and Mg(II), Mn(II), Cu (II) and Zn(II), J. Braz. Chem. Soc. 7 (1996) 239–245, https://doi.org/10.5935/0103-5053.19960038.
[54] R. Corigli, F. Secco, M. Venturini, Equilibriums and kinetics of complex formation at gallium(III). Evidence for an associative mode of activation, Inorg. Chem. 21 (1982) 2992–2998, https://doi.org/10.1021/ic00138a016.
[55] S.D. Cramer, J. Covino, ASM handbook, Corros. Fundam. Test. Prot. 13A (2003).
[56] A.R. Mirak, C.J. Davidson, J.A. Taylor, Study on the early surface films formed on Mg-Y molten alloy in different atmospheres, J. Magnes. Alloy. 3 (2015) 173–179, https://doi.org/10.1016/j.jma.2015.06.003.
[57] A. Samaniego, K. Gusieva, I. Llorente, S. Feliu, N. Birbilis, Exploring the possibility of protective surface oxides upon Mg alloy AZ31 via lutetium additions, Corros. Sci. 89 (2014) 101–110, https://doi.org/10.1016/j.corsci.2014.08.015.
[58] D.N. Shelke, D.V. Jahagirdar, Ternary complexes: equilibrium studies of mixed-ligand complexes of neodymium ion with carboxylic and phenolic acids in aqueous medium, BCSJ 49 (1976) 2142–2147, https://doi.org/10.1246/bcsj.49.2142.
[59] V. Kolhe, K. Dwivedi, Stability constants of mixed ligand complexes of lanthanide (III) and yttrium(III) with complexone and substituted salicylic acids, J. Indian Chem. Soc. 73 (1996) 265–268.
[60] S. Akalin, U.Y. özer, Hydrolysis of Scaq3+ and the stabilities of scandium (III)-Tiron chelates in aqueous solution, J. Inorg. Nucl. Chem. 33 (1971) 4171–4180, https://doi.org/10.1016/0022-1902(71)80517-1.
[61] A.E. Martell, R.M. Smith, NIST Critical Stability Constants of Metal Complexes, NIST database 46, Gaithersburg, MD, USA, 1994.
[62] S.V. Lamaka, D. Höche, R.P. Petrauskas, C. Blawert, M.L. Zheludkevich, A new concept for corrosion inhibition of magnesium: suppression of iron re-deposition, Electrochem. Commun. 62 (2016) 5–8, https://doi.org/10.1016/j.elecom.2015.10.023.